Received 19 January 2024; accepted 3 February 2024. Date of publication 7 February 2024; date of current version 26 February 2024.

Digital Object Identifier 10.1109/OJCOMS.2024.3363423

Indoor Measurements for RIS-Aided Communication: Practical Phase Shift Optimization, Coverage Enhancement, and Physical Layer Security

SEFA KAYRAKLIK [1,2] (Graduate Student Member, IEEE), IBRAHIM YILDIRIM [1,3] (Graduate Student Member, IEEE), IBRAHIM HOKELEK [2,3] (Member, IEEE), YARKIN GEVEZ [1] (Graduate Student Member, IEEE), ERTUGRUL BASAR [1] (Fellow, IEEE), AND ALI GORCIN [2,3] (Senior Member, IEEE)

(INVITED PAPER)

[1]CoreLab, Department of Electrical and Electronics Engineering, Koç University, 34450 Istanbul, Türkiye

[2]Communications and Signal Processing Research Lab., TUBITAK BILGEM, 41470 Kocaeli, Türkiye

[3]Faculty of Electrical and Electronics Engineering, Istanbul Technical University, 34469 Istanbul, Türkiye

CORRESPONDING AUTHOR: S. KAYRAKLIK (e-mail: skayraklik21@ku.edu.tr)

This work was supported in part by the THULAB Project and in part by the KDT Joint Undertaking (JU) through StorAIge Project under Grant 101007321. The JU receives support from the European Union's Horizon 2020 Research and Innovation Programme in France, Belgium, Czech Republic, Germany, Italy, Sweden, Switzerland, Türkiye, and National Authority TÜBİTAK under Project 121N350. The work of Ertugrul Basar was supported by TUBITAK under Grant 120E401.

The preliminary version [1] of this work was presented at ICC 2023 in Rome, Italy [DOI: 10.1109/ICC45041.2023.10278759].

ABSTRACT Practical experiments are a crucial step to demonstrate the viability of reconfigurable intelligent surface (RIS)-empowered communication, which is one of the emerging technologies for next-generation networks. In this paper, we present practical measurements to demonstrate the RIS capabilities for enhancing signal coverage and providing physical layer security (PLS) in an indoor environment. First, extensive measurements are performed in a single-user deployment using iterative, grouping, and codebook-based phase shift optimization methods. The iterative method achieves approximately 10 dB performance improvement in the received signal power through careful adjustments of RIS phase configurations when the receiver is placed at different locations. The grouping method reduces the training time to find a suitable RIS configuration by sacrificing only a few dBs in the received signal power. Another set of experiments is conducted for a multi-user deployment to exhibit PLS, where the RIS is partitioned into two regions serving the intended and unintended users. The results demonstrate that the codebook method can effectively boost the secrecy capacity on the move without utilizing feedback other than the users' positions during the phase shift optimization process, while the iterative method requires a continuous feedback channel for the received signal powers.

INDEX TERMS Reconfigurable intelligent surface, indoor measurements, physical layer security, 6G.

I. INTRODUCTION

NEXT generation applications such as Internet-of-Everything, holographic telepresence, massive twinning, industrial robots, and autonomous vehicles require proactively studying cutting-edge technologies and developing the proof of concepts for sixth-generation (6G) wireless networks [2]. Considering the overarching vision of 6G, a momentous paradigm shift is needed, marking the transition from the traditional understanding of "connected things" to an era characterized by "connected intelligence" [2]. This crucial transformation raises a host of stringent pre-requisites, most notably, extremely high data transmission rates, which is anticipated to reach the unprecedented level of 1 Tb/s. Simultaneously, there is a significant focus on

ultra-high energy efficiency that facilitates the operation of battery-independent devices connected to the intelligent network. The pursuit of 6G also emphasizes the need for extremely low latency and ultra-high reliability [3]. Utilizing advanced physical (PHY) layer techniques such as ultra massive multiple-input multiple-output (MIMO) systems, index modulation (IM), TeraHertz (THz) frequency bands (over 100 GHz), and reconfigurable intelligent surfaces (RISs) can potentially be the way out to meet these highly demanding requirements of 6G. The RIS consisting of a large number of low-cost and passive element arrays, is one of the promising 6G technologies for enhancing link capacity and energy efficiency, minimizing interference, strengthening secure communication, and extending the coverage [4], [5], [6], [7], [8].

The majority of the studies in the literature are based on simulation and theoretical approaches [9], [10], [11], [12], [13], [14], [15], [16], [17], [18]. After highlighting the role of RISs in enhancing 6G network performance, it is important to acknowledge their practical challenges. One example study in [16] provides powerful insights by demonstrating the effects of phase error, hardware impairments, and mobile co-channel interferers on the system performance, such as coverage probability and ergodic capacity in $\kappa - \mu$ fading channels. A novel channel estimation protocol is proposed for RIS-assisted multi-user millimeter wave (mmWave) MIMO systems [17]. In another study [18], a deep reinforcement learning approach is applied to optimize the RIS configuration for multi-user OFDMA systems. The practical experiments are typically avoided due to high expenses of developing or acquiring the RIS prototypes along with the supplementary hardware, including software-defined radios (SDRs) and antennas. In addition, the measurement experiments require significant engineering resources and time for defining the scenarios, setting up the equipment, optimizing the RIS configuration, and ensuring interoperability with the standard communication protocols. However, practical experiments and field tests are crucial steps to demonstrate the practical viability of an emerging technology such as RIS in next-generation network operations.

A set of RIS prototype developments and experimental studies has been conducted to investigate realistic transmission scenarios of RISs [19], [20], [21], [22], [23], [24], [25], [26], [27]. For example, [19] proposes a custom-developed continuous phase-shifted RIS operation in an indoor environment, where continuous phase surfaces provide more degrees of freedom than discrete phase shifts for altering radio patterns owing to more tunable phases. The authors also reports the received power performance of the user placed at different locations and angles with respect to the RIS in an L-shaped indoor environment. Similarly, an RIS is deployed for coverage enhancement purposes in another L-shaped indoor test scenario having only a non-line-of-sight channel [20]. The authors provide the received power performance of the users equipped with monopole and horn antennas, where each unit cell of the custom-made RIS hardware has a 3-bit phase resolution. Furthermore, the performance of binary unit cells to control mmWave beamforming in both near-field and far-field conditions is investigated in [21]. The same 1-bit RIS is utilized as a passive access point extender for mmWave communications in [22]. Four-state reflection in sub-6 GHz frequencies is studied in [23]. Instead of discrete phase shift designed schemes, [24] implements a continuous phase reflecting scheme driven by a varactor-controlled surface. Reference [25] investigates omni-scope transmission exploiting the joint progress of reflective and refractive features of RIS. Reference [26] presents a cutting-edge RIS design that uses RF switch-based technology to enable nearly passive 3D beamforming in the absence of active RF components. With 3-bit resolution and validation using high spatial resolution codebooks, their method surpasses conventional constraints and represents a substantial advancement in wireless communication systems. In [27], a novel RIS prototype with 1100 controllable elements running at 5.8 GHz is tested in indoor and outdoor environments and successfully transmits data over 500 meters. It achieves a 26 dB power gain there, breaking through a concrete wall 30 cm thick. Outside, it achieves a 27 dB power gain. In order to provide intelligent reflection without changing communication standards, this study develops an algorithm for effective RIS configuration.

Recent measurement experiments using RIS prototypes have been reported in [28], [29], [30], [31], [32]. The path loss models of RIS-assisted wireless communication systems operating at 2.6 GHz in outdoor environments are studied in [28]. In [29], a transmissive RIS prototype consisting of 2-bit elements is developed for increased data rates, lower transmit power consumption, and better transmission performance over obstacles. A gap between theoretical research and real-world applications is filled in [30] by providing a comprehensive channel measurement dataset generated using an open-source RIS prototype. Reference [31] introduces a novel user-controlled RIS-assisted system, where the users are able to customize the RIS configuration according to their preferences and locations. Lastly, [32] presents the practical implementation of an RIS-assisted deep learning-based spectrum sensing system, where the secondary user's sensing performance is improved by the RIS.

The RIS technology's practical benefits for multi-user scenarios are demonstrated through practical measurements [33], [34]. The authors propose a novel framework for the RIS by integrating the generalized approximate message-passing algorithm with a sparse channel modeling in [33]. Their work results in a successful real-world implementation of a RIS-assisted multi-user system using SDRs. This system demonstrates impressive gains in the received power of up to 26.6 dB and spectral efficiency of 13.48 bps/Hz, highlighting the transformative potential of RIS in multi-user wireless communication scenarios. Reference [34] studies the physical layer security (PLS) application of the RIS for indoor wireless networks through practical measurement

TABLE 1. Comparison of recent experimental RIS studies.

Key Contents		[28]	[29]	[30]	[31]	[32]	[33]	[34]	[1]	This Work
Deployment	Single-User	✓	✓	✓	✓	✓			✓	✓
	Multi-User						✓	✓		✓
Nature of Study	Theoretical / Simulation		✓			✓		✓		
	Practical Implementation	✓	✓	✓	✓	✓	✓	✓	✓	✓
Optimization Method	Iterative		✓	✓		✓	✓	✓	✓	✓
	Grouping								✓	✓
	Codebook				✓				✓	✓
	Geometric	✓		✓						
Application	Coverage Enhancement				✓				✓	✓
	Physical Layer Security							✓		✓
	Quality of Service		✓				✓			
	Channel Characterization	✓		✓						
	Spectrum Sensing					✓				
Environment	Indoor		✓	✓	✓	✓	✓	✓	✓	✓
	Outdoor	✓								

experiments. The study shows the efficacy of the RIS in improving the secrecy capacity between the transmitter and the intended user while preventing the unintended user from eavesdropping on the reflected signal.

In our current study, we significantly advance our previous work [34] by adopting a codebook-based approach in the application of an RIS for physical layer security. While [34] centered on joint optimization and performance characterization of an RIS at a single point, our latest research innovates by dividing the RIS into two distinct sections for the intended and unintended users, coupled with a codebook approach. This strategy enables a fine grained control and optimization of the RIS, resulting in an enhanced ability for showcasing the versatility and potential of RIS technology in complex scenarios.

Table 1 summarizes the recent experimental RIS studies, which are discussed in the literature review in terms of the deployment, nature of the study, optimization method, application, and environment.

The above-mentioned studies show that the practical applications of the RIS are typically restricted by its computational burden and complexity for determining a suitable phase shift configuration. This limitation is exacerbated when the users are mobile, where the phase shifts of the RIS elements need to be configured timely and dynamically. Assuming that the RIS-assisted wireless communication systems utilize passive reflecting elements, this study comprehensively presents the pros and cons of practical phase shift optimization methods, namely iterative, grouping, and codebook, in an indoor measurement environment for single and multi-user deployments. In the iterative method, possible phase shift states of the first element are applied sequentially to determine the state that yields the maximum received signal power at the receiver, and the same procedure is individually repeated for each of the remaining elements. Note that the received signal power information for each iteration needs to be reported as a performance indicator during the optimization procedure. In the grouping method, the RIS elements are divided into multiple sub-groups for the phase adjustment process, where the same phase shift state is applied to all elements within the same sub-group. In the codebook method, a set of RIS configurations is computed and recorded for pre-determined locations, and the RIS configuration corresponding to the closest location to the receiver terminal is timely applied. For single-user measurement experiments, the iterative method increases the received signal power by around 10 dB when the receiver is positioned at various locations and angles with respect to the RIS. Grouping the RIS elements reduces the training time to find a suitable RIS configuration by sacrificing only a few dBs in the received signal power. In another set of measurement experiments, we present a practical PLS application for mobile users by incorporating a codebook design into the RIS, which is partitioned into two regions serving the intended and unintended users. The measurement results indicate that the codebook method can effectively boost the secrecy capacity without utilizing feedback other than the users' positions during the phase shift optimization process when the users are on the move.

The organization of the paper is as follows. Section II presents the system and signal models. The practical optimization methods, namely iterative, grouping, and codebook, for obtaining a suitable RIS phase shift configuration are described in Section III. The single-user and multi-user measurement experiments are reported in Sections IV and V, respectively. Finally, Section VI concludes the paper.

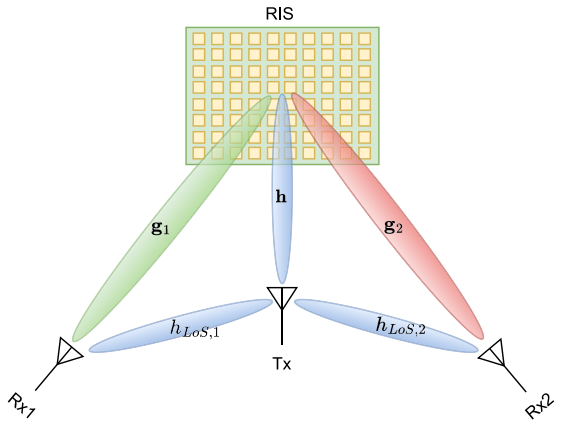

FIGURE 1. A basic RIS-aided wireless communication system for multi-user deployment.

II. SYSTEM AND SIGNAL MODEL

As illustrated in Fig. 1, we consider a basic wireless communication system where the RIS assists the signal transmission from a single-antenna transmitter (Tx) to single-antenna receivers (Rxs). The RIS has the form of a uniform planar array (UPA) with $N = N_x \times N_y$ elements such that each element can add binary phase shifts of either 0° or 180° when the incoming signal is reflected. The wireless channels from the Tx to the RIS and from the RIS to the Rx_i are defined as $\mathbf{h} \in \mathbb{C}^N$ and $\mathbf{g}_i \in \mathbb{C}^N$, respectively. The direct line-of-sight (LoS) channel between the Tx and Rx_i nodes is described as $h_{LoS,i} \in \mathbb{C}$. Suppose that $x[k]$ is a complex baseband signal sent from the Tx, the received signal of Rx_i, $r_i[k]$, can be written as

$$r_i[k] = \left(\mathbf{g}_i^H \boldsymbol{\Theta} \mathbf{h} + h_{LoS,i}\right) x[k] + n_i[k] \tag{1}$$

where $n_i[k] \sim \mathcal{N}_{\mathbb{C}}(0, \sigma_n^2)$ represents the noise at the Rx_i, and $\boldsymbol{\Theta}$, defined as $\text{diag}\{\alpha_1 e^{j\phi_1}, \ldots, \alpha_N e^{j\phi_N}\}$, represents the RIS configuration matrix whose diagonal entries denote the phase shift states of the RIS elements. Since the RIS prototype used in the measurements has passive and binary-phased elements, α_n is constant and ϕ_n takes the values of only 0° and 180°. Furthermore, the LoS component of the received signal is neglected since horn antennas, whose half beamwidth is 40°, are used to transmit and receive signals as depicted in Fig. 3 and Fig. 11. Therefore, the direct link between the Tx and Rx terminals is out of the beamwidth of the antennas.

The primary purpose of using an RIS is to increase the signal-to-noise ratio (SNR) at the receiver by enabling anomalous reflections from the RIS, thereby enhancing the signal coverage. Neglecting the LoS link between the Tx and Rx_i terminals due to the non-intersecting antenna beams, the SNR, which is proportional to the end-to-end gain $|\mathbf{g}_i^H \boldsymbol{\Theta} \mathbf{h}|^2$, can be increased by properly setting the RIS configuration matrix $\boldsymbol{\Theta}$. Therefore, the optimum configuration matrix ($\boldsymbol{\Theta}^*$) maximizing the end-to-end gain for a single-user deployment can be determined as follows:

$$\boldsymbol{\Theta}^* = \arg\max_{\phi_n, \forall n} \left|\mathbf{g}_i^H \boldsymbol{\Theta} \mathbf{h}\right|^2 \quad \text{s.t. } \phi_n \in \{0°, 180°\}, \quad \forall n. \tag{2}$$

The PLS is considered to demonstrate the RIS application for a multi-user deployment in a wireless communication system, where the configuration of the RIS is optimized according to the secrecy capacity. Assuming that the intended and unintended users have approximately the same noise powers, the secrecy capacity, C_s, is expressed in terms of the received signal powers of the intended and unintended users as follows [34]

$$C_s = \max\left(\log_2(P_i) - \log_2(P_u), 0\right), \tag{3}$$

where P_i and P_u represent the received signal powers at the intended and unintended users, respectively. Note that a higher secrecy capacity can be obtained by increasing the intended user's received signal power while decreasing the unintended user's. With the derived secrecy capacity for practical measurements, the optimum configuration matrix ($\boldsymbol{\Theta}^*$), which maximizes the secrecy capacity, can be determined as follows

$$\boldsymbol{\Theta}^* = \arg\max_{\phi_n, \forall n} C_s \quad \text{s.t. } \phi_n \in \{0°, 180°\}, \quad \forall n. \tag{4}$$

III. PRACTICAL PHASE OPTIMIZATION METHODS

In this section, we present three different practical phase shift optimization methods for single and multi-user deployment of RIS-assisted wireless communication systems. The details of the iterative method, which requires feedback from the users through the iterations, the grouping strategy, which reduces the number of iterations during the iterations, and the codebook method, on which the pre-recorded codewords are applied to the RIS without the need for constant feedback during the iterations, are provided to be utilized in the measurement experiments.

A. ITERATIVE METHOD

The configuration of the RIS, which directs the reflected beam towards the Rx, is determined by changing the states of the elements and observing the received signal power for each iteration. Since all possible RIS configurations of 4^{76} are prohibitively expensive to be applied, an iterative method [22] is utilized to find a suitable RIS configuration that provides incoming signals to be reflected towards a desired direction, instead of an exhaustive algorithm. Initially, all elements are set to OFF, indicating that the RIS is in no-phase-shift mode. Then, four possible states of the first element are applied sequentially, and the RIS element is kept in the state that yields the maximum received signal power at the Rx. After determining the best state of the first element, the same procedure is individually repeated for each of the remaining elements. For the RIS prototype consisting of 76 elements, the number of all possible states is equal to 4^{76}.

Algorithm 1 Iterative Method

Input: P_r, N, and S
Output: *States*

```
1: initialize States of the RIS elements to OFF
2: P_max ← 0
3: for i = 1 to N do
4:    for j = 1 to S do
5:       apply state j to ith element
6:       measure P_r
7:       if (P_r > P_max) then
8:          update States
9:          P_max ← P_r
10:      end if
11:   end for
12: end for
13: return States
```

The pseudo-code of the iterative phase adjustment method is given in Algorithm 1, where the measured received power and the maximum received power are denoted as P_r and P_{max}, respectively. Also, N and S denote the total number of reflecting elements on the RIS and the possible number of phase shift states for a reflecting element, respectively. The total number of iterations to determine the phase shift configuration of the RIS depends on N and S. *States* in Algorithm 1 has $N \times S$ different RIS configurations to be explored through the iterations. Therefore, the complexity of the iterative method is linearly proportional to $N \times S$.

As depicted in Algorithm 1, the iterative method requires the measurements of the received signal powers as feedback from the receiver to evaluate the fitness of the RIS configuration at every iteration. The measurement of the receiver signal power corresponding to single iteration takes approximately several hundreds milliseconds. The total time required to explore $N \times S = 76 \times 4$ *States* in Algorithm 1 takes more than one minute. In addition, if this feedback information is received through the control channels of the standards, the signalling over-head also becomes a burden when the number of RIS elements increases. Since the complexity of the iterative method has a linear relationship with $N \times S$, the iterative approach may become impractical for possible 6G applications including mobility scenarios, where some hundreds of RIS elements are utilized.

Algorithm 1 can also be utilized for multi-user scenarios of the RIS-assisted PLS system by only modifying the lines of 6, 7, and 9 as follows: At the 6th line, C_s is measured instead of P_r, and it is compared with C_{max}, which is the maximum secrecy capacity obtained through the iterations, and at the 9th line, C_{max} is updated if the current C_s is higher. Note that C_s is calculated by assuming the availability of the received signal powers for both the intended and unintended users. Although the assumption for the availability of the unintended user's received signal power may not be practical for a real-world implementation of a PLS system, this study aims to demonstrate the potential of the RIS for the PLS application through the measurement experiments. Therefore, Algorithm 1 utilizes the measurements obtained from both the intended and unintended users. However, it is an open issue to calculate the secrecy capacity for the real deployment when the unintended user does not provide its received signal power.

B. GROUPING STRATEGY

The processing time of the iterative method to determine the RIS configuration increases proportionally with the number of RIS elements. The increasing number of RIS elements will also increase the reconfiguration overhead of the RIS. Therefore, one of the useful strategies for finding a suitable RIS configuration is to divide the RIS elements into multiple sub-groups in the phase adjustment process, where the same phase shift is applied to all elements within the same sub-group. In this way, the number of iterations is reduced from the number of elements to the number of sub-groups, and hence, the amount of time spent during the training process of the iterations to generate the suitable RIS configuration will be reduced accordingly.

Let G represent the number of RIS elements in a group. Then, there are $\lceil \frac{N}{G} \rceil$ different groups, where the last group contains only the last remaining RIS elements if $\frac{N}{G}$ is not an integer. The same procedures of the iterative method in Algorithm 1 are applied in the grouping method; however, N is replaced by $\lceil \frac{N}{G} \rceil$. Note that four possible states of the first group are applied sequentially, and the RIS elements of the first group are kept in the same state, which yields the maximum received signal power at the Rx. After determining the best state of the first group, the same procedure is individually repeated for each of the remaining groups. Therefore, the 3rd line of Algorithm 1 is modified by replacing N with $\lceil \frac{N}{G} \rceil$ for the grouping method. The 5th line of Algorithm 1 is modified as "apply state j to the elements of the ith group".

C. CODEBOOK METHOD

The RIS configuration needs to be adjusted on the move within the channel coherence time when the channel characteristics are time-varying. The iterative method in Algorithm 1 assumes that the channels are stationary for the time interval required for iteratively searching all the RIS elements. A long process time of Algorithm 1 prevents switching from one optimized RIS configuration to another within a short time window. In the codebook method, a set of RIS configurations is computed and recorded for pre-determined locations, and the RIS configuration corresponding to the closest location to the receiver terminal is timely applied. Furthermore, employing the codebook method for the RIS configurations eliminates the dependency of the feedback channel between the Rx and the RIS. In other words, the codebook-based approach requires only the geometric positions or the departure/arrival angles of the

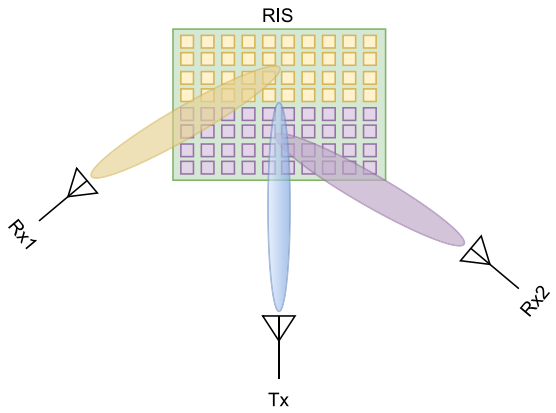

FIGURE 2. Partitioning the RIS into two regions for two-user deployment.

Algorithm 2 Codebook Generation Method

Input: P_r, N, S, and C
Output: Codebook
1: **for** $i = 1$ to C **do**
2: place the Rx at the desired codeword's angle
3: Codebook[i] $\leftarrow$ *Algorithm1*(P_r, N, S)
4: **end for**
5: **return** Codebook

terminals. The pseudo-code of the codebook generation is provided in Algorithm 2, where C is the total number of codewords to be included in a codebook.

Algorithm 2 can be implemented to compose codewords for multi-user scenarios of the RIS-aided PLS system by some alterations. Since there exist at least two users, as intended and unintended, in a basic PLS system, the RIS should serve both users. Therefore, the number of reflecting elements of the RIS is equally partitioned for each user. For example, the RIS is divided into two parts for two-user deployment, which is shown in Fig. 2, as Rx1 and Rx2 indicate the intended and unintended users of a basic PLS system, respectively. Two distinct codewords for each reference location are generated by assigning one half to the intended user to increase its received signal power and the other half to the unintended user to decrease its received signal power. After obtaining the codebook for the intended and unintended user, the actual RIS configuration that is applied to provide secure communication is acquired by combining the corresponding halves of the RIS configuration for the geometric locations or the departure/arrival angles of the intended and unintended users.

IV. SINGLE-USER MEASUREMENT EXPERIMENTS

In this section, we present three different use cases under the same measurement setup of RIS-assisted wireless communication for a single-user deployment. The performance of the RIS configuration methods, namely iterative, grouping, and codebook, is reported using an RIS prototype for various indoor wireless communication scenarios.

TABLE 2. Hardware specifications of the experimental setup.

Hardware	Description
Transceiver	ADALM-PLUTO SDR, adjusted to operate at 5.2 GHz to convey over-the-air signals.
RIS	Greenerwave prototype working at 5.2 GHz with 76 reflecting elements, each having adjustable phase shifts of 0° and 180° for both polarization.
Antenna	Horn antennas with a directivity of 13 dBi and a half power beamwidth of 30° at the 5 GHz frequency band.

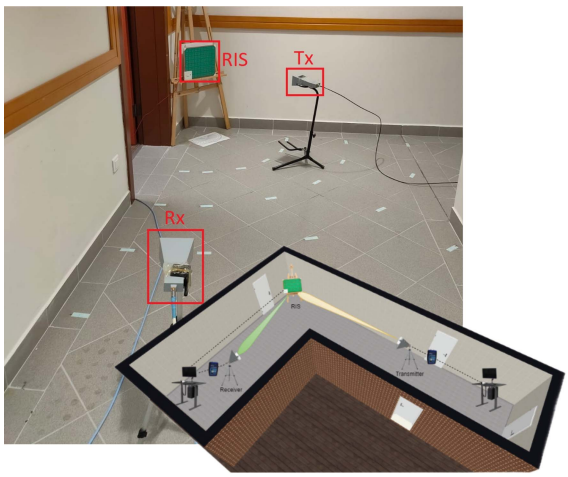

FIGURE 3. The measurement setup of the RIS-aided wireless communication system in an indoor office environment.

A. MEASUREMENT SETUP

An RIS-assisted measurement setup for a single-user wireless communication system is illustrated in Fig. 3, where two ADALM-PLUTO software-defined radios (SDRs) are utilized for transmission and reception of over-the-air signals, $x[k]$, in an L-shaped hallway of an indoor office environment. The RIS is mounted on the hallway's corner, while the antennas of the Tx and Rx SDRs are positioned at various angles and distances from the center of the RIS throughout the measurement process. The RIS prototype developed by Greenerwave [35] is used to focus the transmitted signal in the desired direction through software-controlled phase shifts. The working bandwidth of the RIS is 1 GHz around the center frequency of 5.2 GHz. The RIS has a UPA structure with a 10×8 element grid, yet the right corner of the 2×2 part is preserved for its controller, ending up with a total of 76 reflecting elements. The PIN diodes are used to adjust the reflection coefficient of the elements by configuring their phase shifts as 0° or 180°. Furthermore, each element includes two PIN diodes corresponding to horizontal and vertical polarization, resulting in four possible states. The summary of equipment utilized in the measurement experiments of the RIS-assisted wireless communication system is provided in Table 2.

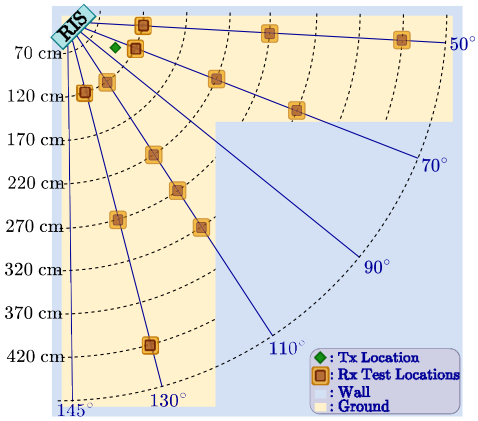

FIGURE 4. The top view of the setup with all Rx test locations.

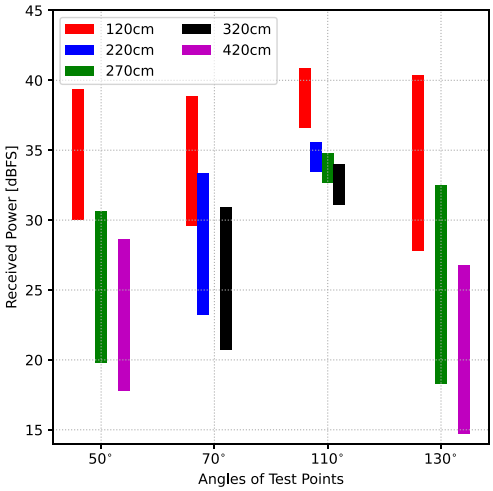

FIGURE 5. The received power measurements for various locations of the user.

The setup in Fig. 3 aims to enhance the indoor coverage by increasing the received signal power through the deployment of an RIS. In the transmission and reception of the signals, horn antennas provide control over the direction of the signals, while the measurement environment of an L-shaped hallway prevents a direct link between the Tx and Rx SDRs. The hallway is partitioned into grids with respect to the angles, defined clockwise from the RIS surface as $\{50°, 70°, 90°, 110°, 130°, 145°\}$, and the distances from the RIS as $\{120, 170, 220, 270, 320, 420\}$ cm. As shown in Fig. 4, the intersections of the angle and distance lines denote our grid representation used in the practical measurements. The Tx SDR is placed on a fixed location at 78°, and 100 cm directed to the RIS while the Rx SDR's antenna emulating a mobile user is moved among the grid points according to the measurement scenarios.

During the measurement experiments, the Tx SDR sends a single-tone sinusoidal signal of 100 kHz at the carrier frequency of 5.2 GHz towards the RIS using a horn antenna, and the reflected signal from the RIS reaches the Rx SDR to measure the received signal power at 5.2 GHz. In Algorithm 1, the received power is calculated by using the time samples captured at the center frequency of 5.2 GHz and moved to the complex baseband by the Rx SDR. Since the SDR has a 12-bit analog-to-digital converter, the sampled complex baseband signals can be represented as integers in the range of $(-2047, 2048]$. Therefore, the received signal power is computed in the decibels relative to full scale (dBFS) via the equation:

$$P_{dBFS} = 10\log_{10}\left(\frac{1}{K}\sum_{k}^{K}|r[k]|^2\right) \tag{5}$$

where P_{dBFS} denotes the average power of the received complex baseband signal $r[k]$, and the total number of received samples is K.

B. USE CASE 1: PHASE ADJUSTMENT WITH ITERATIVE METHOD

In the first set of experiments, the received power of the Rx SDR at different angles and distances is measured to report the performance improvement of the RIS iterative method in an indoor environment. During the experiments, the RIS is controlled with a Python script, which takes a Boolean array of 152 elements corresponding to the horizontal and vertical polarization states of the PIN diodes. In the Boolean array, 0 and 1 correspond to no-phase-shift and 180°-phase-shift mode, respectively. The sampling rate of the Tx and Rx SDR are set to 1 MHz. The buffer size of the Rx SDR, the number of time samples to calculate the received signal power, is selected as 10000.

Fig. 5 shows the measurement results of the received signal power for the Rx SDR at 13 different locations, which are illustrated in Fig. 4 as brown squares, when the iterative method in Algorithm 1 is applied to obtain the RIS configuration. For example, the green bar for the angle of 50° in Fig. 5 illustrates that the received signal power is around 20 dBFS at the beginning of the iterations, and it increases by 11 dB and reaches approximately 31 dBFS at the end of the iterations. As clearly seen in Fig. 5, the RIS performances at different distances for the same angle exhibit similar patterns of enhancements on the received signal power. In fact, the increase in the received signal power is around 10 dB for the angles of 50° and 70° and approximately 12 dB for the angles of 130°. For the case of 110°, the RIS can only boost the received signal power by around 4 dB since the Rx SDR has higher received signal power because of the symmetrical position of the Rx with respect to the Tx.

C. USE CASE 2: PHASE ADJUSTMENT WITH GROUPING STRATEGY

In the second set of experiments, the grouping method for a joint phase adjustment is utilized to reduce the training time for determining a suitable RIS configuration. Fig. 6 (b), (c), and (d) show the examples of the sub-grouped RIS configurations when the sub-groups of two, four, and eight elements are used, respectively. Note that the figures

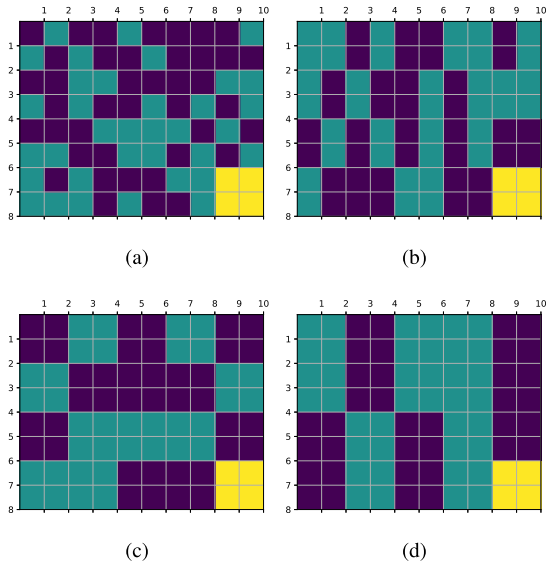

FIGURE 6. Example RIS configurations of (a) one-by-one, (b) two-by-two, (c) four-by-four, and (d) eight-by-eight grouping.

illustrate the states of the RIS for only one polarization and Fig. 6 (a) does not utilize the grouping strategy.

The received signal powers for the Rx angles of 70°, 90°, 130°, and 145° at 170 cm through the iterations of Algorithm 1, which are obtained from the grouped elements, are shown in Fig. 7. The given plots demonstrate the impact of grouping with two, four, and eight elements with respect to the increasing iteration.

Fig. 7 illustrates that the groups of two and four elements mostly perform close to the one-by-one adjustment case. For instance, even at 90°, the group of eight elements increases the received signal power by around 3 dB less than the single-element iterations. For the most of the angles, the groups of two and four elements accomplish very close received signal power, within a few dB, in comparison to the one-by-one case. Thus, employing the grouping approach would significantly reduce the time and effort required to optimize the RIS configurations.

D. USE CASE 3: PHASE ADJUSTMENT WITH CODEBOOK METHOD

In the final set of experiments for the single-user deployment, the performance of the codebook method is compared with the iterative method, where the pre-computed RIS configurations are timely applied when the Rx SDR's antenna is moved to pre-determined test points. In this approach, a codebook containing codewords of the RIS configurations for 6 different angles at 170 cm is generated using Algorithm 2 to be used afterward. The example codewords of the horizontal PIN diodes on/off configurations are shown in Fig. 8, where the purple color represents the no-phase-shift mode of the RIS, the green color indicates the 180°-phase-shift mode, and the yellow color corresponds to the RIS controller, which has no reflecting elements.

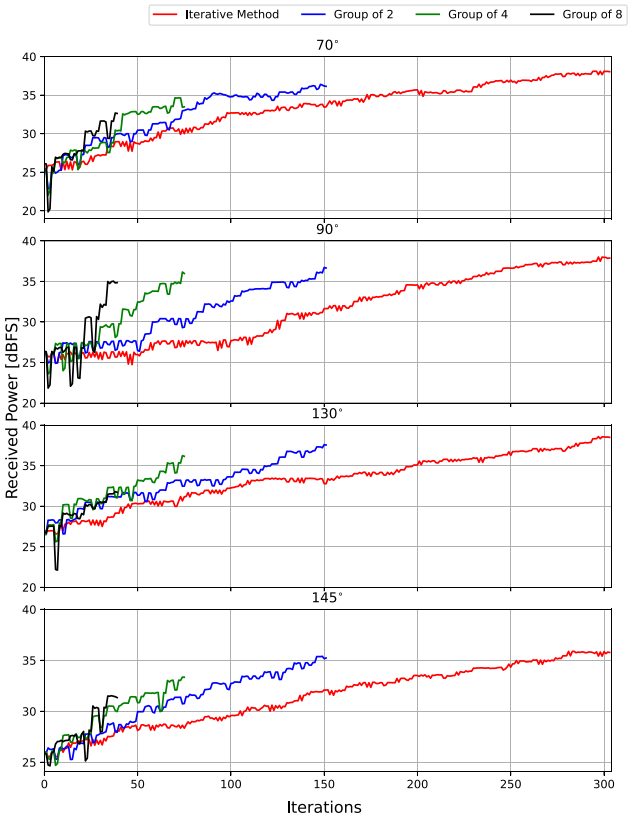

FIGURE 7. The received signal power for the iterative and grouping methods, where $G = \{2, 4, 8\}$ for the grouping approach.

For the measurement experiments, the Rx SDR's antenna is moved along the test points at the interior regions of the grids. Fig. 9 illustrates its path along the hallway, where the brown squares denote the measurement locations of the codebook method as the mobile Rx moves while the pink circles represent the locations of the pre-computed RIS configurations that maximize the received power. The codebook is generated by recording these pre-computed RIS configurations (codewords) for the corresponding purple circles. During the movement of the Rx SDR's antenna, the codeword of the purple circle, which has the closest distance to the current brown square of the receiver, is applied to the RIS. The received signal powers are measured for three cases: (i) the RIS is in no-phase-shift mode (RIS-off), (ii) the offline pre-computed codewords are applied to the RIS (Offline Codeword), and (iii) the configuration of the online iterative method in Algorithm 1 is applied to the RIS (Online Iterative).

Fig. 10 shows the received signal powers of the mobile Rx at 10 different locations for three cases. Without loss of generality, the results show that the lowest received power results are measured when the RIS is off while the online iterative method provides the highest results. The RIS configured with the codewords keeps the received signal powers above 30 dBFS for all locations. Furthermore, the received powers of the codebook method gets closer

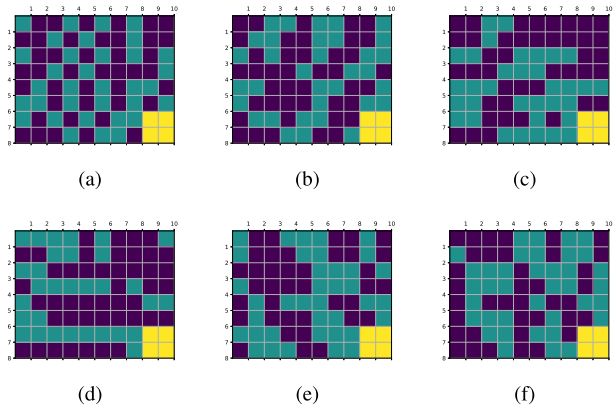

FIGURE 8. The codewords of the horizontal PIN diodes on/off configurations at the distance of 170 cm, and the angles of (a) 50°, (b) 70°, (c) 90°, (d) 110°, (e) 130°, and (f) 145°.

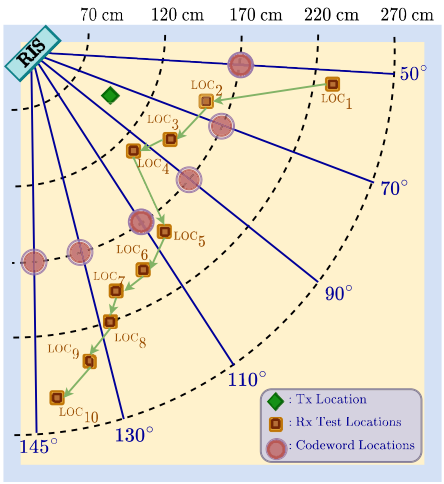

FIGURE 9. The top view of the RIS-assisted transmission setup for various Rx test and codeword locations.

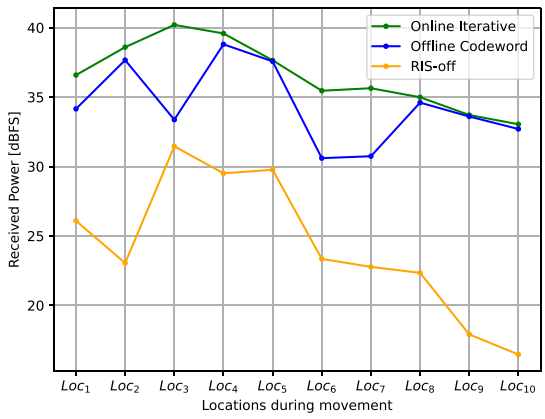

FIGURE 10. The received signal power measurements when the Rx is on the move.

to the results of the online iterative configurations when the angles of the measurement locations get closer to the angles of the pre-computed codewords. Therefore, the RIS using the offline codebook approach can achieve comparable performance results, which are approximately 3 dB lower

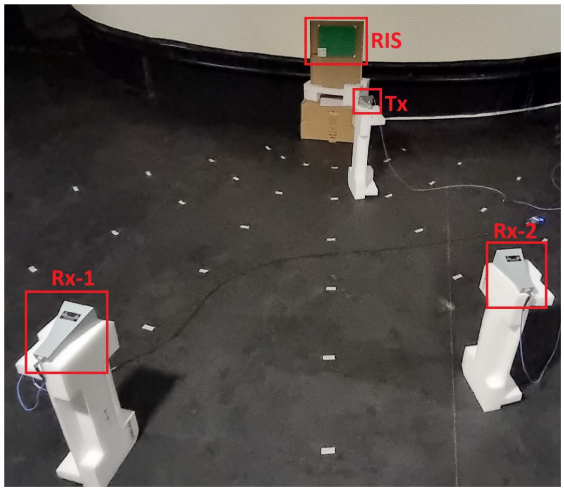

FIGURE 11. The measurement setup of the RIS-aided PLS system for multi-user deployment in an indoor environment.

than the real-time iterative method, without going through many iterations of Algorithm 1. It takes approximately 1 ms to switch from one codeword to another in the RIS [21]. Accordingly, the codebook approach becomes a viable alternative to support time-varying channel conditions if the mobile user's location can be accurately predicted.

V. MULTI-USER MEASUREMENT EXPERIMENTS

In this section, we present the measurement setup and results of RIS-assisted wireless communication for a multi-user deployment. We consider the RIS's passive beamforming ability to provide PLS, where the RIS boosts the received signal power of the intended user Rx1 while the unintended user Rx2 is prevented from receiving the reflected beams. The performances of the codebook-based method and the iterative method with the joint optimization parameter are analyzed for two measurement scenarios of mobile users of Rx1 and Rx2 with different paths.

A. MEASUREMENT SETUP

The RIS-aided measurement setup of a multi-user wireless communication system is shown in Fig. 11, where the measurement experiments are conducted in an empty room by utilizing three ADALM-PLUTO SDRs to transmit and receive over-the-air signals, $x[k]$. The same RIS prototype, which is described in the previous section, is employed along with one Tx and two Rx SDRs through the measurement campaigns. The Tx SDR transmits a 100 kHz single-tone sinusoidal signal at the center frequency of 5.2 GHz. The horn antenna of the Tx SDR is directed towards the RIS, which illuminates the Rx1 and Rx2 SDRs with its reflected beams. The empty room is divided into a grid according to the angles and distances from the RIS as depicted in Fig. 12 and Fig. 13. The Tx SDR antenna is placed on a fixed location at 78° and 105 cm while the antennas of Rx1 and Rx2 SDRs representing two mobile users move around according to the paths in Fig. 12 and Fig. 13 during

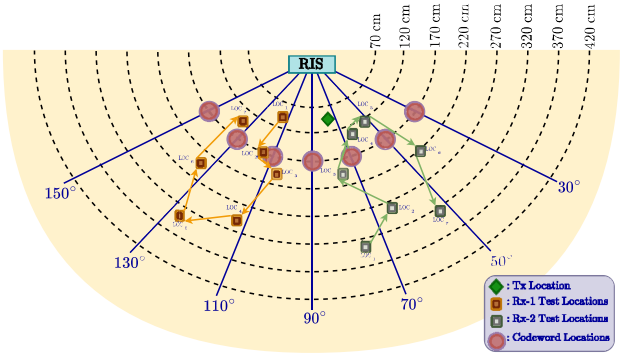

FIGURE 12. The top view of the RIS-assisted multi-user transmission scenario when Rx1 and Rx2 are on the move with similar patterns.

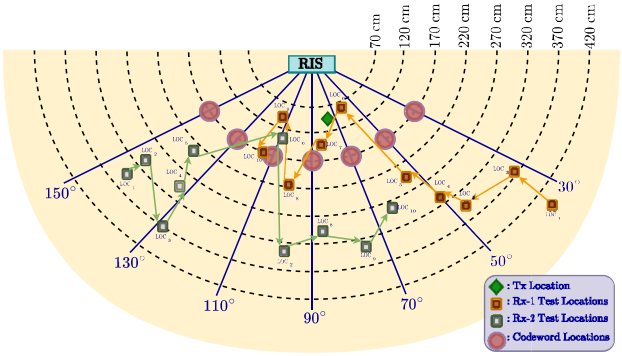

FIGURE 13. The top view of the RIS-assisted multi-user transmission scenario when Rx1 and Rx2 are on the move with opposite directions.

the measurement experiments. The pink circles indicate the codeword locations of the RIS configurations, while the brown and green squares denote the measurement locations of Rx1 and Rx2, respectively. Note that there are two different measurement scenarios. The aim of the first scenario in Fig. 12 is to observe the performance of the RIS for various distances at similar angles. The objective of the second scenario in Fig. 13 is to inspect the RIS's performance for a wide range of angles and distances.

During the measurement experiments, the secrecy capacity is calculated using (3), where the intended and unintended users are assumed to have the same noise powers. In order to validate this assumption, 11400 measurement experiments are conducted using the SDRs of Rx1 and Rx2 to record their noise powers [34]. Fig. 14 demonstrates the noise power densities of Rx1 and Rx2, which exhibit similar behavior. The difference of the mean values for the noise power densities is measured around 0.228 dB. Therefore, the accuracy of the secrecy capacity calculation is slightly affected by this assumption, where all the phase shift optimization methods utilizes the same expression. During the measurement experiments, the secrecy capacity is calculated using (3) except the *max* operator. Since the unintended user's received signal power can be higher than the intended user's throughout the measurement path when the RIS is turned off, the *max* operator for preventing the

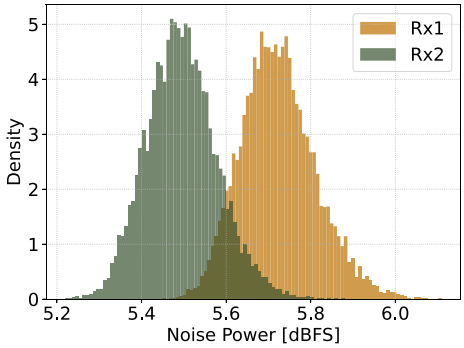

FIGURE 14. Noise power densities of Rx1 and Rx2 [34].

secrecy capacity from being negative is ignored in order to demonstrate the performance improvement of the RIS even if the unintended user is placed much closer to the transmitter. The negative secrecy capacity values should be treated as 0. Therefore, the formulation used through the measurements is given in the following expression:

$$C_s = 0.1 \log_2(10)(P_i - P_u). \tag{6}$$

Since the received signal powers are measured and computed using (5) and the capacity is computed with $\log_2$, the correction coefficient is added to the above formulation.

B. PERFORMANCE RESULTS FOR PHYSICAL LAYER SECURITY

The efficient codebook design of the RIS's configurations is implemented for the RIS-aided multi-user wireless communication system. The whole RIS is partitioned into two parts, with one serving Rx1 and the other serving Rx2. Therefore, a codebook for Rx1 containing codewords for the configurations of the first half of the RIS at all the grid angles of 170 cm distance is generated to boost the received signal power of Rx1 as the intended user. Then, another codebook containing the codewords of the other half for Rx2 in the same locations is formed to decrease the received signal power of Rx2 as the unintended user. Five corresponding codewords for 38 elements of the RIS are recorded for each location specified above since the same performance of the codewords cannot be achieved when the codewords for Rx1 and Rx2 are combined and applied to the RIS. Therefore, the best combination of the codewords of Rx1 and Rx2 are selected from the five codewords of Rx1 and Rx2.

For the first scenario of the measurement experiments, Rx1 and Rx2 move along various distances at similar angles, whose path is given in Fig. 12, to inspect the performance of the RIS for providing PLS in a wireless communication system. During the movement of Rx1 and Rx2, the combined codewords corresponding to the closest reference points are applied to provide secure communication through the RIS-assisted PLS system by increasing the Rx1's received signal power while decreasing the Rx2's. Similar to Section IV-D, the received signal powers of Rx1 and Rx2 are measured and

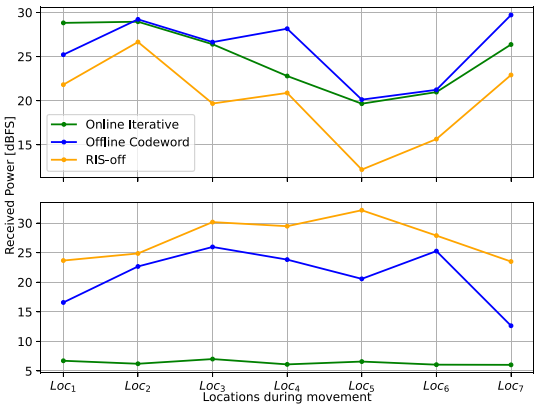

FIGURE 15. The received signal power measurements of Rx1 (top) and Rx2 (bottom) for the first scenario of the RIS-assisted PLS system.

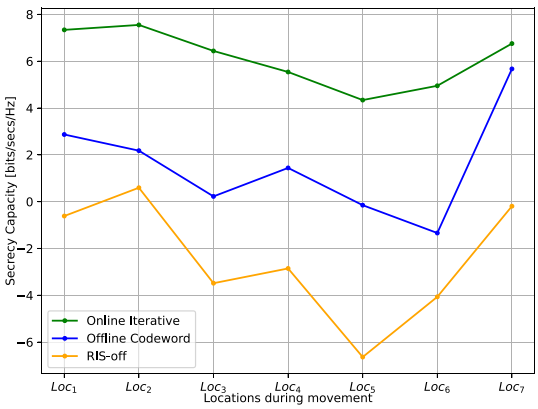

FIGURE 16. The secrecy capacity for the first scenario of the RIS-assisted PLS system.

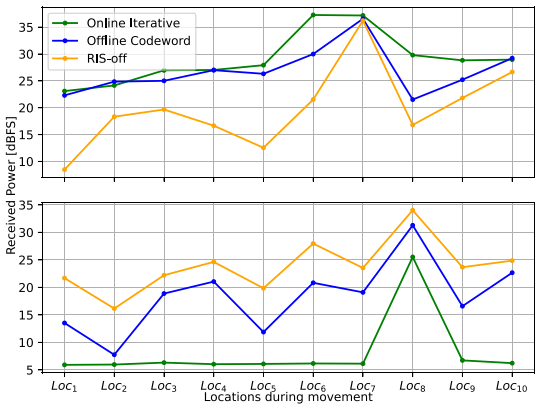

FIGURE 17. The received signal power measurements of Rx1 (top) and Rx2 (bottom) for the second scenario of the RIS-assisted PLS system.

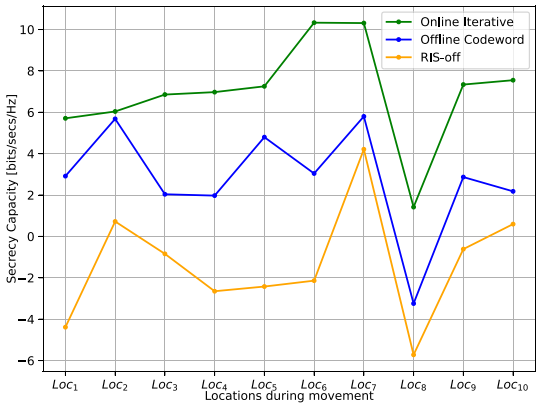

FIGURE 18. The secrecy capacity for the second scenario of the RIS-assisted PLS system.

compared for the three cases, such as the RIS is in no-phase-shift mode, the offline codewords of the recorded codebook, and the configuration of the online iterative method, which is optimized via Algorithm 1 on the test point. Fig. 15 shows the change in the received signal powers of Rx1 and Rx2 at the top and bottom plots, respectively, through the seven test points.

It can be observed from Fig. 15 that both the iterative and codebook approaches boost the received signal of Rx1 and decrease the received signal of Rx2. The offline codeword method for Rx1 performs slightly better than the online iterative method since the iterative method behaves equally to Rx1 and Rx2 through their joint optimization; therefore, the improvement obtained from Rx2 being pushed into the noise floor is much higher than Rx1.

In order to evaluate the RIS's performance under the codebook method for the PLS problem, the secrecy capacity, which is computed using (6), through the test location is given in Fig. 16. As can be seen from Fig. 16, the codebook approach improves the secrecy capacity above the zero level for most of the locations. In addition, the online iterative method with joint optimization for Rx1 and Rx2 performs better than the codebook approach since it can lower the Rx2's received signal power to the noise floor. However, the iterative method requires feedback from both the receivers, yet the codebook method only needs the angle information.

For the second scenario of the measurements, Rx1 and Rx2 move along a wide range of angles and distances, whose path is given in Fig. 13, to observe the RIS's performance in the RIS-aided PLS communication system. The same measurement procedure of the previous scenario is followed in this scenario. Fig. 17 illustrates the change of the received signal powers of Rx1 and Rx2 at the top and bottom plots, respectively, through the ten test points.

It can be observed from Fig. 17 that both the iterative and codebook approaches exhibit a similar behavior for the received signal powers of Rx1 and Rx2, where both the iterative and codebook methods increase the Rx1's received signal powers and degrade the Rx2's received signal power as both Rx1 and Rx2 move according to their pre-defined paths resulting in a variety of angles and distances as depicted in Fig. 13. However, the RIS cannot provide much improvement in the Rx1's received signal power at the 7th location since its received signal power is already high when the RIS is off. In addition, the RIS is unable to reduce the Rx2's received signal power to the noise floor at the

8th location since its power is already high due to the reflected signals even when the RIS is off. Note that the clockwise angles from the RIS for these two positions of Rx1 at the 7th location and Rx2 at the 8th location are very close to each other. It can be concluded that the RIS performs poorly for the placements of these Rx1 and Rx2 locations since the reflected signals from the RIS illuminate the corresponding clockwise angle even when the RIS is off.

The secrecy capacity through the test location of the second scenario is shown in Fig. 18. It can be observed from Fig. 18 that the codebook approach keeps the secrecy capacity above 2 bps/Hz except for the 8th location. The secrecy capacity for the 8th location remains below zero since the RIS is not capable of decreasing the received signal power of Rx2 into the noise floor.

VI. CONCLUSION

In this study, the practical measurements of RIS-aided wireless communication systems in an indoor environment have been conducted to enhance the signal coverage for a single-user deployment and provide secure communication for a multi-user deployment. We utilize the iterative, grouping, and codebook-based methods as the practical phase shift optimization of the RIS elements. For all experiments, the iterative method provides performance improvement, while the training time to find a suitable RIS configuration using the grouping method is significantly reduced by sacrificing only a few dBs in the received signal power. The results indicate that the iterative algorithm provides a practical solution for reconfiguring the RIS elements when the channel characteristics do not rapidly change. As the coherency time of the channel decreases, the grouping strategy provides a suitable alternative by balancing the trade-off between the performance and the configuration time. In the second set of experiments, the codebook method is applied to increase the secrecy capacity in the PLS application for a multi-user deployment, where the RIS is partitioned into two parts serving the intended and unintended users. The results demonstrate that when the number of RIS elements is high and the receivers are mobile, the codebook approach may be the only alternative to provide timely switching among the RIS configurations. The performance optimization of the codebook configuration is fairly high as it is determined through an offline process; however, the performance degradation may occur due to either inaccurate localization of the receivers or the lack of the codebook configurations for all possible locations. The results of our measurement campaigns provide these powerful insights regarding the practical application of RIS phase shift optimization methods for both coverage enhancement and PLS scenarios. The future work will study the theoretical analysis of the performance metric including the secrecy capacity under different SNR values when the RIS is either off or configured with various phase shift optimization approaches.

REFERENCES

[1] S. Kayraklık, I. Yildirim, Y. Gevez, E. Basar, and A. Görçin, "Indoor coverage enhancement for RIS-assisted communication systems: Practical measurements and efficient grouping," in *Proc. IEEE Int. Conf. Commun.*, May 2023, pp. 485–490.

[2] K. B. Letaief, W. Chen, Y. Shi, J. Zhang, and Y.-J. A. Zhang, "The roadmap to 6G: AI empowered wireless networks," *IEEE Commun. Mag.*, vol. 57, no. 8, pp. 84–90, Aug. 2019.

[3] R. Gupta, D. Reebadiya, and S. Tanwar, "6G-enabled edge intelligence for ultra-reliable low latency applications: Vision and mission," *Comput. Stand. Interfaces*, vol. 77, Aug. 2021, Art. no. 103521.

[4] I. Yildirim, A. Uyrus, and E. Basar, "Modeling and analysis of reconfigurable intelligent surfaces for indoor and outdoor applications in future wireless networks," *IEEE Trans. Commun.*, vol. 69, no. 2, pp. 1290–1301, Feb. 2021.

[5] Y. Liu et al., "Reconfigurable intelligent surfaces: Principles and opportunities," *IEEE Commun. Surveys Tuts.*, vol. 23, no. 3, pp. 1546–1577, 3rd Quart., 2021.

[6] E. Basar, I. Yildirim, and F. Kilinc, "Indoor and outdoor physical channel modeling and efficient positioning for reconfigurable intelligent surfaces in mmWave bands," *IEEE Trans. Commun.*, vol. 69, no. 12, pp. 8600–8611, Dec. 2021.

[7] E. Basar, "Reconfigurable intelligent surface-based index modulation: A new beyond MIMO paradigm for 6G," *IEEE Trans. Commun.*, vol. 68, no. 5, pp. 3187–3196, May 2020.

[8] I. Yildirim, A. Koc, E. Basar, and T. Le-Ngoc, "RIS-aided angular-based hybrid beamforming design in mmWave massive MIMO systems," in *Proc. IEEE Global Commun. Conf.*, 2022, pp. 5267–5272.

[9] A. Subhash, A. Kammoun, A. Elzanaty, S. Kalyani, Y. H. Al-Badarneh, and M.-S. Alouini, "Optimal phase shift design for fair allocation in RIS-aided uplink network using statistical CSI," *IEEE J. Sel. Areas Commun.*, vol. 41, no. 8, pp. 2461–2475, Aug. 2023.

[10] J. Hu, Y.-C. Liang, and Y. Pei, "Reconfigurable intelligent surface enhanced multi-user MISO symbiotic radio system," *IEEE Trans. Commun.*, vol. 69, no. 4, pp. 2359–2371, Apr. 2021.

[11] B. Di, H. Zhang, L. Song, Y. Li, Z. Han, and H. V. Poor, "Hybrid beamforming for reconfigurable intelligent surface based multi-user communications: Achievable rates with limited discrete phase shifts," *IEEE J. Sel. Areas Commun.*, vol. 38, no. 8, pp. 1809–1822, Aug. 2020.

[12] B. Di, H. Zhang, L. Li, L. Song, Y. Li, and Z. Han, "Practical hybrid beamforming with finite-resolution phase shifters for reconfigurable intelligent surface based multi-user communications," *IEEE Trans. Veh. Technol.*, vol. 69, no. 4, pp. 4565–4570, Apr. 2020.

[13] C. Huang, R. Mo, and C. Yuen, "Reconfigurable intelligent surface assisted multiuser MISO systems exploiting deep reinforcement learning," *IEEE J. Sel. Areas Commun.*, vol. 38, no. 8, pp. 1839–1850, Aug. 2020.

[14] X. Gan, C. Zhong, C. Huang, and Z. Zhang, "RIS-assisted multi-user MISO communications exploiting statistical CSI," *IEEE Trans. Commun.*, vol. 69, no. 10, pp. 6781–6792, Oct. 2021.

[15] H. Zhang, B. Di, Z. Han, H. V. Poor, and L. Song, "Reconfigurable intelligent surface assisted multi-user communications: How many reflective elements do we need?" *IEEE Wireless Commun. Lett.*, vol. 10, no. 5, pp. 1098–1102, May 2021.

[16] A. Sikri, A. Mathur, and G. Kaddoum, "Joint impact of phase error, transceiver hardware impairments, and mobile interferers on RIS-aided wireless system over κ-μ fading channels," *IEEE Commun. Lett.*, vol. 26, no. 10, pp. 2312–2316, Oct. 2022.

[17] J. Chen, Y.-C. Liang, H. V. Cheng, and W. Yu, "Channel estimation for reconfigurable intelligent surface aided multi-user mmWave MIMO systems," *IEEE Trans. Wireless Commun.*, vol. 22, no. 10, pp. 6853–6869, Oct. 2023.

[18] X. Yuan, S. Hu, W. Ni, R. P. Liu, and X. Wang, "Joint user, channel, modulation-coding selection, and RIS configuration for jamming resistance in multiuser OFDMA systems," *IEEE Trans. Commun.*, vol. 71, no. 3, pp. 1631–1645, Mar. 2023.

[19] A. Araghi et al., "Reconfigurable intelligent surface (RIS) in the sub-6 GHz band: Design, implementation, and real-world demonstration," *IEEE Access*, vol. 10, pp. 2646–2655, 2022.

[20] J. Rains et al., "High-resolution programmable scattering for wireless coverage enhancement: An indoor field trial campaign," *IEEE Trans. Antennas Propag.*, vol. 71, no. 1, pp. 518–530, Jan. 2023.

[21] J.-B. Gros, V. Popov, M. A. Odit, V. Lenets, and G. Lerosey, "A reconfigurable intelligent surface at mmWave based on a binary phase tunable metasurface," *IEEE Open J. Commun. Soc.*, vol. 2, pp. 1055–1064, 2021.
[22] V. Popov et al., "Experimental demonstration of a mmWave passive access point extender based on a binary reconfigurable intelligent surface," *Front. Commun. Netw.*, vol. 2, Oct. 2021, Art. no. 733891.
[23] L. Dai et al., "Reconfigurable intelligent surface-based wireless communications: Antenna design, prototyping, and experimental results," *IEEE Access*, vol. 8, pp. 45913–45923, 2020.
[24] R. Fara, P. Ratajczak, D.-T. Phan-Huy, A. Ourir, M. Di Renzo, and J. De Rosny, "A prototype of reconfigurable intelligent surface with continuous control of the reflection phase," *IEEE Wireless Commun.*, vol. 29, no. 1, pp. 70–77, Feb. 2022.
[25] H. Zhang et al., "Intelligent omni-surfaces for full-dimensional wireless communications: Principles, technology, and implementation," *IEEE Commun. Mag.*, vol. 60, no. 2, pp. 39–45, Feb. 2022.
[26] M. Rossanese, P. Mursia, A. Garcia-Saavedra, V. Sciancalepore, A. Asadi, and X. Costa-Perez, "Designing, building, and characterizing RF switch-based reconfigurable intelligent surfaces," in *Proc. 16th ACM Workshop Wireless Netw. Testbeds Exp. Eval. CHaracterization*, 2022, pp. 69–76.
[27] X. Pei et al., "RIS-aided wireless communications: Prototyping, adaptive beamforming, and indoor/outdoor field trials," *IEEE Trans. Commun.*, vol. 69, no. 12, pp. 8627–8640, Dec. 2021.
[28] J. Lan et al., "Measurement and characteristic analysis of RIS-assisted wireless communication channels in sub-6 GHz outdoor scenarios," in *Proc. IEEE 97th Veh. Technol. Conf. (VTC-Spring)*, 2023, pp. 1–6.
[29] J. Tang, M. Cui, S. Xu, L. Dai, F. Yang, and M. Li, "Transmissive RIS for B5G communications: Design, prototyping, and experimental demonstrations," *IEEE Trans. Commun.*, vol. 71, no. 11, pp. 6605–6615, Nov. 2023.
[30] S. Tewes, M. Heinrichs, K. Weinberger, R. Kronberger, and A. Sezgin, "A comprehensive dataset of RIS-based channel measurements in the 5GHz band," in *Proc. IEEE 97th Veh. Technol. Conf. (VTC-Spring)*, 2023, pp. 1–5.
[31] E. Arslan, F. Kilinc, E. Basar, and H. Arslan, "Network-independent and user-controlled RIS: An experimental perspective," 2023, *arXiv:2308.07646*.
[32] S. Kayraklik, I. Yildirim, E. Basar, I. Hokelek, and A. Gorcin, "Practical implementation of RIS-aided spectrum sensing: A deep learning-based solution," 2023, *arXiv:2307.14985*.
[33] Z. Zhou, H. Yin, L. Tan, R. Zhang, K. Wang, and Y. Liu, "Multi-user beamforming in RIS-aided communications and experimental validations," 2023, *arXiv preprint arXiv:2309.09460*.
[34] S. Keşir, S. Kayraklık, İ. Hökelek, A. E. Pusane, E. Basar, and A. Görçin, "Measurement-based characterization of physical layer security for RIS-assisted wireless systems," in *Proc. IEEE 97th Veh. Technol. Conf. (VTC-Spring)*, Jun. 2023, pp. 1–6.
[35] Greenerwave. Paris, France. 2023. [Online]. Available: https://greenerwave.com/

SEFA KAYRAKLIK (Graduate Student Member, IEEE) received the B.Sc. (with High Hons.) degree in electrical and electronics engineering from Bogazici University, Istanbul, Türkiye, in 2021, and the M.Sc. degree in electrical and electronics engineering from Koc University, Istanbul, Türkiye, in 2023, where he is currently pursuing the Ph.D. degree. He is also a Researcher with HİSAR Lab., TUBITAK BILGEM. His research interests include reconfigurable intelligent surfaces and spectrum sensing.

IBRAHIM YILDIRIM (Graduate Student Member, IEEE) received the B.S. and M.S. degrees from Istanbul Technical University, Türkiye, in 2017 and 2019, respectively. He is currently pursuing the Ph.D. degree with Koç University.

He is currently a Research and Teaching Assistant with Istanbul Technical University. His current research interests include MIMO systems and reconfigurable intelligent surfaces. He received the Exemplary Reviewer Award of the IEEE TRANSACTIONS ON COMMUNICATIONS in 2021. He is also a co-recipient of the Best Paper Award from the IEEE LATINCOM 2020. He has been serving as a Reviewer for IEEE JOURNAL ON SELECTED AREAS IN COMMUNICATIONS, IEEE TRANSACTIONS ON COMMUNICATIONS, IEEE TRANSACTIONS ON VEHICULAR TECHNOLOGY, and IEEE COMMUNICATIONS LETTERS.

IBRAHIM HOKELEK (Member, IEEE) received the B.Sc. and M.Sc. degrees in electrical and electronics engineering from Bilkent University, Ankara, Türkiye, and the Ph.D. degree from the Graduate Center, The City University of New York. He worked as a Senior Research Scientist with Telcordia Technologies, Inc., Piscataway, NJ, USA. He has been working as a Project Manager and the Chief Researcher with the Scientific and Technological Research Council of Turkiye. He has been serving as an Adjunct Professor with the Electronics and Communication Engineering Department, Istanbul Technical University. His research interests include IP networks, wireless mobile networks, network planning and management, and deterministic networks. He received full scholarships during his B.Sc. and M.Sc. studies at Bilkent University.

YARKIN GEVEZ (Graduate Student Member, IEEE) received the B.S. degree in electrical and electronics engineering from the Yeditepe University, Istanbul, Turkiye, in 2019, and the M.Sc. degree from the University of Ontario, Institute of Technology Toronto, Canada, in 2020. He is currently pursuing the Ph.D. degree in electrical and electronics engineering with Koc University, Istanbul, Türkiye. His research interests include wireless communications, reconfigurable intelligent surfaces, and deep learning techniques for 5G and beyond wireless networks.

ERTUGRUL BASAR (Fellow, IEEE) received the Ph.D. degree from Istanbul Technical University in 2013. He is currently an Associate Professor with the Department of Electrical and Electronics Engineering, Koç University, Istanbul, Türkiye, and the Director of the Communications Research and Innovation Laboratory. He is the author/coauthor of around 150 international journal publications and ten patents that received more than 12K citations. His primary research interests include beyond 5G and 6G wireless networks, communication theory and systems, reconfigurable intelligent surfaces, index modulation, waveform design, and signal processing for communications. In the past, he served as an Editor/Senior Editor for many journals, including IEEE COMMUNICATIONS LETTERS from 2016 to 2022, IEEE TRANSACTIONS ON COMMUNICATIONS from 2018 to 2022, *Physical Communication* from 2017 to 2020, and IEEE ACCESS from 2016 to 2018. He is currently an Editor of *Frontiers in Communications and Networks*. He is a Young Member of the Turkish Academy of Sciences in 2017.

ALI GORCIN (Senior Member, IEEE) received the B.Sc. and M.Sc. degrees from Istanbul Technical University and the Ph.D. degree in wireless communications from the University of South Florida. After working with the Scientific and Technological Research Council of Turkiye (TÜBİTAK) as a Researcher for more than six years, he moved to the U.S. to pursue his Ph.D. degree. He worked with Anritsu Company during his tenure with USF and worked with Reverb Networks and Viavi Solutions after his graduation. He is currently an Assistant Professor with Istanbul Technical University. He is also the President of TÜBİTAK BİLGEM.